https://doi.org/10.1139/cgj-2019-0460

Small strain shear modulus and damping ratio of two unsaturated lateritic sandy clays

Authors: C. W. W. Ng, O. T. Bentil and C. Zhou*

*Corresponding author

Author's affiliation and address:

Name: Charles Wang Wai Ng

Title: CLP Holdings Professor of Sustainability

Affiliation: Department of Civil and Environmental Engineering, The Hong Kong University of Science and Technology, Clear Water Bay, Kowloon, Hong Kong

Email: cecwwng@ust.hk

Name: Obed Takyi Bentil

Title: PhD Student

Affiliation: Department of Civil and Environmental Engineering, The Hong Kong Polytechnic University, Hung Hom, Kowloon, Hong Kong

Email: o-t.bentil@connect.polyu.hk

Name: Chao Zhou

Title: Assistant Professor

Affiliation: Department of Civil and Environmental Engineering, The Hong Kong Polytechnic University, Hung Hom, Kowloon, Hong Kong

Email: c.zhou@polyu.edu.hk

ABSTRACT

In this study, resonant column tests carried out to investigate the influence of suction on the shear modulus and damping ratio of two compacted lateritic sandy clays from Ghana (GL) and Nigeria (NL) are reported. Each type of soils was tested under two confining pressures and at three suctions. The microstructure of the soils was also studied through a scanning electron microscope. It is found that the effects of suction on maximum shear modulus (G_0) are about 10% larger for GL than NL, mainly due to the existence of smaller aggregates in GL. Moreover, an increase in suction from 0 to 300 kPa for both soils resulted in a lower elastic threshold shear strain, different from the behaviour of other soils reported in the literature. The uniqueness of lateritic soils is likely attributed to their high sesquioxide content and much larger aggregates, which shrink upon an increase in suction. Drying of specimens from 0 to 300 kPa resulted in an increase of about 22% and 100% in initial damping ratio (D_0) for GL and NL, respectively. The difference in D_0 for GL and NL and is attributed to larger aggregation of NL because of its higher iron sesquioxide content, leading to more cladding.

KEYWORDS:

Dynamic properties; Lateritic soil; Sesquioxide, Suction; Unsaturated; Microstructure

INTRODUCTION

Lateritic soil is a chemically weathered soil widely distributed in tropical and subtropical regions (Netterberg 2014). The formation of a lateritic soil (i.e. laterization) results in the reduction of silica and the increasing concentration of iron and aluminium sesquioxides (Blight 1991). This process generates iron nodules or cemented aggregates, because of the different polarity of the surface charges of clay and sesquioxides. (Gidigasu 1976; Airey et al. 2012). These aggregates would affect the hydromechanical properties of the lateritic soils (e.g. Miguel and Bonder 2012; Ng et al. 2019). Lateritic soils are usually unsaturated and are extensively used in the construction of many geotechnical structures such as railway embankment, foundation and retaining wall. Coincidentally, a significant number of countries located in these tropical regions are areas of medium to high seismicity (Pineda et al. 2014). Therefore, it is necessary to investigate the dynamic behaviour of lateritic soils at unsaturated states.

The shear modulus (G) and damping ratio (D) at small strains are very important fundamental parameters for predicting the dynamic response of geotechnical structures. Several studies thus far have suggested that these dynamic properties are affected by a number of parameters (e.g. confining pressure, void ratio, plasticity, structure, suction, degree of saturation, compaction water content, gradation, and sample disturbance) (Wu et al. 1984; Seed et al. 1986; Vucetic and Dobry 1991) whereas the G/G_0–γ and D–γ curves are less sensitive to these parameters (Vinale et al. 1999; Xenaki and Athanasopoulos 2008). The influence of suction on G_0 of unsaturated soils has been well recognised (Mancuso et al. 2002; Vassallo et al. 2007; Ng and Yung 2008; Sawangsuriya et al. 2009; Khosravi and McCartney 2012; Heitor et al. 2013; Hoyos et al. 2015). On the other hand, very little is known about the relation between suction and the normalised shear modulus (G/G_0) as well as the elastic threshold shear strain of unsaturated soils (Ng and Xu 2012; Ng et al. 2017). The research relative to the dynamic response of geomaterials has been focused mostly on sedimentary soils (Pineda et al.

2014). However, there is evidence that materials from residual soils with cementing agents (sesquioxides) in the soil structure show contradictory results due to their different microstructures.

The objective of this study is to investigate the dynamic behaviour of unsaturated compacted lateritic soils. As far as the authors are aware, this is the first study of the small strain shear modulus and damping ratio of unsaturated compacted lateritic soils. Different from the behaviour of other unsaturated soils reported in the literature, the behaviour of unsaturated lateritic soils is influenced by their high content of sesquioxide (i.e. iron and aluminium oxides) which causes significant particle aggregation. No attention has been given by previous researchers to investigate the influence of sesquioxide composition on soil behaviour. In this paper, two lateritic soils with similar total sesquioxide content but different contents of iron and aluminium oxides are studied and compared. This is important because with the same total sesquioxide content but different iron and aluminium oxide content, their microstructure and dynamic properties are expected to be different.

TESTING SOILS AND SPECIMEN PREPARATION

Two soils, sampled from Nigeria (NL) and Ghana (GL), were tested in this study. Figure 1 shows their particle size distributions, which were determined using ASTM (2017a, 2017b) with and without the use of dispersant for the wet and dry sieving, respectively. For each soil, the difference between the wet and dry sieving curves is due to the aggregation of fine particles. NL and GL are classified as sandy lean clay (CL) and sandy fat clay (CH), respectively, according to the Unified Classification System (ASTM 2017c). Figure 2 shows the Proctor compaction curves of the two soils. Table 1 summarizes the index properties, the optimum compaction conditions as well as the chemical composition of these two soils. X-ray diffraction (XRD) results confirmed the presence of quartz, hematite, and kaolinite as the common main

mineral components in the two different soils. However, in NL there is the presence of goethite whiles in GL there is the presence of halloysite. Moreover, NL is different from GL in terms of chemical compositions, which were determined through X-ray fluorescence (XRF) tests. It can be seen that there is higher iron oxide content for NL than GL. With regards to aluminium sesquioxides content, NL is lower than GL. These differences are likely to influence the microstructure as well as the dynamic properties. More discussion on the basis of measured microstructures and macro behaviour is given later. In addition, the total content of the sesquioxide for NL and GL is 38% and 36%, respectively. With this sesquioxide content, these two soils are both classified as lateritic soils (Netterberg 2014).

It is well recognized that the microstructure and hence dynamic behaviour of lateritic soils are greatly affected by the sesquioxide content, which is the sum of iron and aluminium contents (Goldberg 1989; Airey et al. 2012). For the same sesquioxide content, the fractions of iron and aluminium oxides could be different. The effects of the different amounts of the two oxides on the microstructure and dynamic behaviour have not studied. Hence, the two lateritic soils were tested and compared in this study to investigate the influence of iron and aluminium contents. The major mineral contents of these two soils are representative of the lateritic soils widely distributed in West Africa (Lyon Associates and BRRI 1971). They have almost the same sesquioxide content with a difference less than 2%, but consist of very different iron and aluminium oxide contents.

Statically compacted specimens were prepared for the soils at 19.5% water content and 1.62 g/cm^3 dry density as indicated in Figure 2. The two lateritic soils were compacted at the same water content and to the same density. This is because the compaction water content and density affect the size of aggregates formed during specimen preparation (Tarantino 2011). Moreover, due to the presence of iron and/or aluminium sesquioxides, the formation of aggregations is significant in lateritic soils (Zhang et al. 2016). This compaction method allows

for investigating the influence of sesquioxide content on the aggregation and the possible influence of compaction water content and density is eliminated.

The initial suction of the compacted specimens was determined using the null-test axis translation technique. The initial suction of the compacted NL and GL specimens are 150 kPa and 170 kPa, respectively.

Figure 3 shows drying water retention curves of the compacted NL and GL soils, measured using a pressure plate apparatus (Tawiah 2019). The measured SWRC was fitted with the model by Fredlund and Xing (1994) with three fitting parameters (i.e. a, n and m). The fitting parameters a, n, and m are 2.22, 7.96 and 0.229 for NL, whereas for GL they are 2.56, 12.67 and 0.183, respectively. The residual water condition was not reached in the SWRC test because only suctions lower than 400 kPa were applied. The air entry value (AEV) for NL and GL is estimated to be 2 kPa and 2.5 kPa, respectively. It can be seen from Figure 3 that the AEVs of these two lateritic soils are very low, even though they are classified as CL and CH, respectively. This is likely because both soils present dual-porosity due to particle aggregation, as supported by the SEM image. The dual-porosity may be missed in the SWRCs due to limited data points. The desorption rate of both NL and GL appears to be similar. From Figure 3, it can be concluded that that GL has a slightly higher water retention ability than NL.

Figures 4 (a) and (b) show the SEM images, which are used for characterising the aggregation and hence for explaining the dynamic properties of the two lateritic soils. In this study, the ImageJ software was used for image processing and analysis. The SEM micrographs were imported into the ImageJ software and binarized to show the aggregates (white) and interaggregate pores (black) (see Figure 4 (c) and (d)). The fraction was estimated from the binarized images for the two lateritic soils. On one hand, NL contains about 36% aggregates and 64% interaggregate pores, whereas GL is made up of 42% aggregate and 58%

interaggregate pores. Compared with GL, NL has more interaggregate pores and its aggregates are less interlocked. On the other hand, the aggregate sizes of lateritic soils are generally larger than other soils, attributed to their iron oxides. As illustrated by Zhang et al. (2016), iron oxides provide cladding effects (i.e. coating on a material) and hence result in larger aggregations of fine particles. Qualitatively, the SEM micro-photographs presented are useful for quantifying the aggregate size and hence for explaining the dynamic properties of the two lateritic soils. In further studies, more microstructural analysis such as MIP tests is needed to fully understand the influence of sesquioxide on aggregation and the dynamic properties of lateritic soils.

TESTING PROGRAMME, APPARATUS AND PROCEDURES

To investigate the small strain behaviour of lateritic soils, 12 resonant column tests were carried out in this study. For each soil, two confining pressures (50 and 100 kPa) were applied, and three suction conditions were considered: as-compacted condition (150 and 170 kPa for NL and GL, respectively), saturated condition (zero suction) and dried condition (300 kPa). Details of the test programme are summarized in Table 2.

The tests were carried out using an energy-injecting virtual mass resonant column equipment (Li et al. 1998). This device is a Drnevich type resonant column apparatus. Figure 5 shows the schematic diagram of the resonant column after Li et al. (1998). The equipment allows for the continuous measurement of shear modulus and damping ratio in a strain range of 0.0005% to 0.03%. In addition, the number of vibration cycles is minimized. Hence, the soil sample disturbance is diminished. Details of the device were reported by Li et al. (1998).

Figure 6 shows the stress paths of the as-compacted, saturated and dried specimens. The as-compacted specimens were directly put on the pedestal of the resonant column apparatus after measuring their dimensions. After attaching a membrane, a low vacuum pressure of about 10 kPa was applied to hold each specimen in place to minimize the soil

disturbance during the installation of resonant column components. The magnet was then placed on the cap platen and other electronic components were arranged. Another series of specimens ('saturated' specimens in Table 2) was set-up in the resonant column apparatus in a similar approach and then saturated by applying a back pressure of 200 kPa. For the dried specimens, their suction was increased to 300 kPa using the axis-translation technique in a pressure plate. Suction equalisation generally took about 7 days in the pressure plate apparatus. After suction equalisation, the specimen was transferred to the resonant column equipment. The initial states of the as-compacted specimen, saturated and dried specimens prior to application of the corresponding confinement are denoted by A_0, A_1 and A_2, respectively. Then, an *effective confining pressure* of 50 kPa (i.e. B_1) or 100 kPa (i.e. C_1) was applied to the specimen for the *saturated condition*. On the other hand, a *net confining pressure* of 50 kPa or 100 kPa was applied to the *as-compacted specimen* (i.e. B_0 or C_0) and *dried condition* (i.e. B_2 or C_2). During the application of cell pressure, the vertical of each specimen was monitored by a linear variable differential transducer (LVDT). The consolidation under a given confinement was considered to be finished when the reading of LVDT reached a constant value. At the end of compression, resonant column torsional shear test was conducted. All the resonant column tests were conducted at constant water condition. Table 2 summarises the testing programme and soil state after application of the corresponding confinement prior to resonant column test.

INTERPRETATIONS OF EXPERIMENTAL RESULTS

Maximum shear modulus of lateritic soils

Figure 7(a) shows the maximum shear modulus (G_0) of NL and GL at a confining pressure of 50 kPa. At zero suction, G_0 values of NL and GL are 54 MPa and 50 MPa, respectively. Their difference may be because GL shows a higher swelling during the saturation process and its density after saturation is slighter lower, as shown in Table 2. When suction increases from 0

to 150 kPa, G_0 value of NL increases from 54 MPa to 73 MPa (35% increase) and then G_0 value increases from 73 MPa to 86 MPa (18% increase) when suction increases from 150 to 300 kPa. For GL, the value of G_0 increases from 50 MPa to 84 MPa (66% increase) when suction increases from 0 to 170 kPa. G_0 value subsequently increases from 84 MPa to 101 MPa (20% increase) when suction increases from 170 to 300 kPa. It is clear that suction effects on G_0 values of GL are more significant than those of NL. This difference is related to the microstructure of these two soils. As illustrated in Figure 4, the size of aggregates and thus inter-aggregate pores of GL are smaller than those of NL. The existence of smaller pores allows GL to retain more water than NL at a given suction. For example, the equilibrium water contents at a suction of 300 kPa are 17.9% and 16.5% for GL and NL, respectively (see Table 2). Thus, there are more air-water interfaces which provide more stabilising effect in GL, resulting in a higher increase rate of G_0 with increasing suction.

Figure 7(b) shows G_0 values of NL and GL at a confining pressure of 100 kPa. At zero suction, G_0 values of NL and GL are 71 MPa and 81 MPa. G_0 values of GL is larger than that of NL by 15%. This is different from the findings at a confining pressure of 50 kPa (see Figure 7(a)), suggesting that stress effects on G_0 are more significant for GL than for NL. The observed difference in stress effects can be explained using SEM images in Figure 4. Due to the existence of smaller aggregations and higher clay content in GL, more inter-aggregate contacts are observed. Hence, an increase in stress would contribute to the increase in G_0 values of GL more than NL because of more aggregate contacts. Also, the void ratio of both soils at zero suction and confining pressures of 50 and 100 kPa (see Table 2) indicates that GL is more compressible than NL. This result is consistent with those of Cha et al. (2014), who suggest that highly compressible fine-grained soils have higher stiffness sensitivity to changes in stress.

It can be seen from Figure 7(a) that when suction increases from 0 to 300 kPa, the moduli of GL and NL increase by about 87% and 54%, respectively. For Figure 7(b), the

moduli of GL and NL increase by about 70% and 60%, respectively. The suction-induced increment in modulus is larger for GL. This is likely because, at a given suction, GL has a higher water content than NL, as shown in Figure 3. As a consequence, GL has more water meniscuses which can enhance contact stress between soil grains leading to an increase in shear modulus. According to Table 2 and Figure 7, the GL soil at the dried state has a higher G_0 but a larger void ratio than that at the compacted state. The difference in void ratio is only 0.004 and 0.007 at 50 kPa and 100 kPa confining pressure, respectively. Hence, the influence of void ratio should be negligible and suction effects play a dominant role. Note that, the soil suction was increased to higher suction before subsequent compression in the RC apparatus. This led to the lower compressibility due to a lower degree of saturation of the dried specimen compared to the as-compacted soil. Hence, the lower compressibility resulted in the dried soil having void ratio slightly higher than the as-compacted soil. The higher G_0 at the dried state is mainly because at a higher suction, the soil specimen is stiffened by water meniscus (Wheeler and Karube 1996).

From Table 2, the difference in void ratio at different suctions is small (less than 0.002). This implies that soil behaviour during the drying/wetting process is essentially elastic and soil states are within the LC curve. Thus, density effects on the G_0 at different suctions would play a very minor role.

Equation (1) was proposed and verified by Ng and Yung (2008) based on extensive data. All of the parameters have very clear physical meaning, as explained above. In the current study, this equation is applied to interpret the experimental results of the two lateritic soils. It should be noted that some other models can be also used to meet this objective, such as several models able to capture the non-linear relationship between suction and stiffness at lower and higher suctions (Vassallo et al. 2007; Sawangsuriya et al. 2008, 2009; Hoyos et al. 2015; Hoyos and Puppala 2017).

$$G_{0(ij)} = C_{ij}\, F(e) \left[\frac{p}{p_r}\right]^{2n} [1 + \frac{(u_a - u_w)}{p_r}]^{2b} \qquad (1)$$

where $G_{0(ij)}$ is the maximum shear modulus at the shear plane *ij*; C_{ij} is a function of soil structure; *F(e)* is a void ratio function; *p* is confining pressure; p_r is a reference stress; u_a - u_w is matric suction; *n* and *b* are fitting parameters. The value of all parameters in equation (1) is calibrated using experimental results in Figure 7 and summarized in Table 3. The calculated G_0 values are also included in the figure for comparisons. It can be seen that the measured and calculated results are well-matched, suggesting that the equation is able to well capture G_0 value of unsaturated soils. On the other hand, among the model parameters, C_{ij} is used to describe the structure of the soil on G_0. The value of this parameter is smaller for NL (310) than GL (320) because of smaller aggregations and smaller inter-aggregates pores in GL, resulting in more stable soil skeleton. This is because of more aluminium oxides in GL than NL. In general, the aluminium oxides have a greater stabilizing effect on the microstructure than the iron oxides (Goldberg 1989). The value of *n* for NL is 0.19 whiles that of GL is 0.25. The higher the value of *n* implies the soil with a larger change in void ratio during compression. Hence, GL is more compressible than NL between 50 kPa to 100 kPa confining stress considered in this study. In the case of *b*, it describes the sensitivity of G_0 values with changes in suction. The value of *b* for NL is 0.17 whereas for GL is estimated as 0.24. In other words, the influence of suction on the G_0 values will be larger for GL than NL. The difference in parameter *b* is likely due to the existence of smaller aggregations and pores of GL than NL, as revealed by SEM images (see Figure 4). Hence, GL is able to hold more water at the same suction of 300 kPa, leading to more meniscus water in GL and thus stiffened the inter-particle contacts of GL than NL.

Figure 8(a) and 8(b) illustrates the changes in G_0 values with confining stress (*p*) at different suctions for NL and GL, respectively. As expected, G_0 value increases with an

increase in confining pressure at all suction conditions. With respect to the parameter *n* and the microstructure of the soils, the higher the value of *n* of GL than NL is because of the many aggregate contacts found in the SEM image of GL. Thus, the influence of stress is observed to be higher in GL than NL due to the existence of many small aggregations and thus more aggregate contacts. Stress effects on the dynamic properties of soils have been extensively studied (Hardin and Black 1966; Vassallo et al. 2007; Ng and Yung 2008; Shankar Kumar et al. 2014; Hoyos et al. 2015 etc), and the reported results show a very consistent trend. Hence, stress effects are not the focus of the current study and only two confining stresses (50 and 100 kPa) are considered.

Shear modulus degradation curves

The shear modulus (G) with increasing shear strain was normalised by the maximum shear modulus (G_0) and is represented as the normalised modulus degradation (G/G_0) curve. At a very small strain range (<0.001%), the shear modulus remains nearly constant and the soil behaves elastically (Simpson 1992). As shear strain increases from a very small strain range (<0.001%) to small strain range (0.001% - 0.1%), the normalised shear modulus reduces drastically. The shear strain value separating these two ranges is called the elastic threshold shear strain. In other words, the elastic threshold shear strain corresponds to the limit of the elastic proportion (Vucetic 1994; Ng and Xu 2012)**.** The experimental data are best-fitted with Ramberg–Osgood model parameters (Borden et al. 1996). This is then used to estimate the elastic threshold shear strain, at G/G_0 = 0.95 (Clayton and Heymann 2001; Ng and Xu 2012). This quantification is used in the discussion of the experimental results presented in this section.

Figure 9(a) shows the G/G_0 degradation curves for NL. It can be seen from this figure that the G/G_0 of NL shifts towards lower shear strain values for 50 kPa confining pressure when

suction increases from 0 to 150 kPa (i.e. NLs p50 to NLc p50). The G/G_0 further moves towards lower shear strain values for NL with an increase in suction to 300 kPa for p50 (i.e. NLd p50). Similarly, at 100 kPa confining pressure, an increase in suction to 300 kPa resulted in a shift of the G/G_0 curve to lower shear strain values for NL.

Regarding GL in Figure 9(b), the G/G_0 curve also shifts to lower shear strain values with an increase in suction to 300 kPa for 50 kPa confining pressure. When confining pressure increases from 50 kPa to 100 kPa (i.e. p100), the G/G_0 for GL similarly decreases with an increase in suction to 300 kPa. For both GL and NL an increase in suction to 300 kPa resulted in a shift of the degradation curve to lower elastic shear strain values. This is due to a change in the elastic threshold shear strain. Moreover, a shift in the G/G_0 towards lower shear strain values could be speculated as a decrease in plasticity (Vucetic and Dobry 1991; Vardanega and Bolton 2013) causing the soil to behave more granular after drying to 300 kPa suction due to the aggregated structure of the NL and GL (see Figure 4). On the contrary, the G/G_0 of an unsaturated CDT at suction of 150 kPa and 300 kPa from a previous study (Ng and Xu 2012) showed that an increase in suction resulted in a shift of the G/G_0 curve to higher shear strain values.

Figure 10 shows changes in elastic threshold shear strain with suction. The elastic threshold shear strain of NL at confining pressure of 50 kPa remains unchanged when suction increases from 0 to 150 kPa. However, the elastic threshold shear strain values for NL decreases with an increase in suction to 300 kPa for p50. Similar to p50, the elastic threshold shear strain at p100 for NL similarly decreases with an increase in suction to 300 kPa. In summary, the elastic threshold shear strain is lower at higher suction of 300 kPa for the two confining pressures considered in this study. Generally, the elastic threshold shear strain for all suction states increases with confining pressure for NL specimens with the exception of NLd.

Regarding GL in Figure 10**,** the elastic threshold shear strain of GL is also lower at higher suction for the two confining pressures considered in this study. When suction increases from 0 to 300 kPa, the elastic threshold shear strains of NL and GL consistently become smaller. This trend is different from that of other fine-grained soils such as completely decomposed tuff (CDT), whose threshold shear strain is larger at a higher suction (Ng and Xu 2012). The unique behaviour of GL and NL is likely because they have a high sesquioxide content (i.e. a large amount of iron and aluminium oxides) and form large-size aggregates. These aggregates shrink upon suction increases, resulting in larger inter-aggregates pores and thus a lower elastic threshold shear strain. The decrease in the elastic threshold value with increasing suction and confining stress is possible due to micro-fissuring., Nevertheless, more studies on the linkage between microstructural features and elastic threshold strain value are required in the future. For other fine-grained soils, an increase in suction would increase the normal force and hence prevent slippage between the soil particles (Wheeler et al. 2003). Consequently, the elastic threshold shear strain becomes larger at a higher suction.

Initial damping ratio

Figure 11 shows the trend of the initial damping ratio (D_0) at a confining pressure of 50 kPa and 100 kPa**.** At a particular confining pressure, D_0 of NL decreases slightly for 0 kPa to 150 kPa followed by a significant increase from 150 kPa to 300 kPa. With respect to GL shown in Figure 11, D_0 remains approximately constant as suction increases at 50kPa and 100kPa confining pressure for GL. In the figure, D_0 is significantly larger when suction increases to 300 kPa for NL.

The relationship between D_0 and confining pressure at a particular suction for NL shows that, generally, the D_0 decreases with confining pressure. Mostly, the D_0 decreases as confining pressure increases with the exception of GLc (s = 170 kPa). The decrease in D_0 with an increase

in confining pressure is consistent with what has been observed by other researchers (Dobry and Vucetic 1987; Senetakis et al. 2013). As summarised in Dobry and Vucetic (1987), the damping ratio stays constant or decrease with confining pressure.

The values of D_0 for NL ranges from 10% to 23% whereas for GL, the D_0 takes values ranging from 11% to 14%. From previous studies, higher values of D_0 have been determined for some special categories of soils, i.e. 14% for soils with cemented bonding, and 9% for compacted soils (Mancuso et al. 1993; Tzyy-Shiou et al. 2001; Kallioglou et al. 2008). Hence, it can be inferred that the presence of iron and aluminium sesquioxides in lateritic soils which causes aggregation to the compacted soil resulted in the high D_0 values obtained in this study. However, the differences between NL and GL implies that the D_0 values of unsaturated GL are less sensitive to suction than NL. For instance, at a confining pressure of 50 kPa, D_0 decrease slightly (about 12% decrease for both soils) when suction increases to 150 or 170 kPa. On the other hand, D_0 increases significantly for NL than GL (i.e. 100% and 22% increase for NL and GL, respectively) during drying to 300 kPa suction. The difference in D_0 for NL and GL after drying to 300 kPa suction is because of the initial microstructure and soil plasticity.

The damping in a soil is the energy dissipation within the material itself, mainly due to microstructural mechanisms (Ashmawy et al. 1995). According to Upreti and Leong (2018), increase confining pressure for saturated soil specimen and increase of suction in unsaturated soil specimen increases the interlocking of the soil grains which reduces the relative movement of the soil particles and lowering damping of the soil specimens. However, changes in suction do not only increase interlocking between soil grains, especially in an aggregated soil structure. Moreover, compacted clayey soils with aggregated structure undergo microstructural changes following wetting–drying hydraulic paths (Romero 2013). Thus, for an aggregated soil, the effects of suction on the soil may also result in the evolution of microstructure together with stiffening of the soil skeleton. With a suction increment from 0 to 300 kPa, the initial damping

ratio (D_0) of NL increased from about 15 to 25%. This is likely because the aggregates of unsaturated soils shrink with an increase in suction (Romero 2013). Consequently, the interlocking between aggregates may be weakened, resulting in an increase in the damping ratio. On the contrary, with the same suction increment, D_0 of GL remained almost constant. The difference between these two soils is likely because the aggregate size of GL is much smaller, as revealed by the SEM images. The smaller aggregations are more interlocked, as revealed by the results of ImageJ analysis. Therefore, suction effects on the damping ratio do not change significantly.

Strain effects on damping ratio at various stresses and suction

Figure 12(a) shows the relations of normalised damping ratio (D/D_0) and shear strain for NL. For p50, the figure illustrates that the D/D_0 shifts towards lower shear strain values when suction increases from 0 to 150 kPa (i.e. NLs p50 to NLc p50) beyond the elastic threshold strain. However, the D/D_0 curve of NLd (s = 300 kPa) is between that of NLd and NLc (s = 0 and 150 kPa, respectively). Regarding p100, similar to p50, the normalised damping ratio of NLd p100 falls between NLs p100 and NLc p100 beyond shear strain of 0.008%.

In the case of GL in Figure 12(b), the D/D_0 curve also shifts to lower shear strain values with an increase in suction to 300 kPa for 50 kPa confining pressure. When confining pressure increases from 50 kPa to 100 kPa (i.e. p100), the D/D_0 for GLs and GLc showed similar patterns. However, for GLd there is a significant shift of D/D_0 to lower shear strain values beyond the elastic threshold shear strain. Consistent with the normalised shear modulus, an increase in suction to 300 kPa resulted in a shift of the normalised damping ratio curve to lower elastic shear strain values for GL. This is due to a change in the elastic threshold shear strain.

Discussion

The dynamic properties of each soil were determined at three different states, i.e. as-compacted, wetting post compaction, and drying post compaction. These three states are not representative of the same hydraulic path. If the soil water retention curve (SWRC) is considered, the as-compacted state corresponds to a point on a scanning curve, whereas saturated and dried states are located on different hydraulic branches due to the hysteretic behaviour of the SWRC. The hydraulic hysteresis would affect the dynamic behaviour of unsaturated soils, as reported by some previous researchers (Ng et al. 2009; Khosravi and McCartney 2012; Khosravi et al. 2018). Consequently, the observed differences in G_0 at the three different states are not only due to suction, but also hydraulic state.

Pineda et al. (2014) investigated the effects of weathering intensity on the dynamic properties of two intact weathered soils (a residual soil and a saprolitic soil) at the saturated state. They determined the microstructure and dynamic response of soil specimens retrieved from different depths within the same weathering profile. They found that the residual soil had greater shear modulus than the saprolitic soil. This difference was attributed to the presence of sesquioxides acting as cementing agents in the residual soil. For each type of soil tested in the current study, the specimens are expected to have the same weathering intensity because they were sampled from the same depth (1 m). It is worthwhile to test lateritic specimens retrieved from different depths within the same weathering profile in future studies, similar to the work of Pineda et al. (2014). Such a test program is useful for assessing effects of weathering degree (i.e., iron oxide content, sesquioxides content, and degree of particle aggregation) on the dynamic properties of the same lateritic soil in an unsaturated state.

Indeed, subjecting lateritic soil specimens to shear strain levels between 0.01% and 0.1% may have induced some changes in the original structure of the soil (degree of particle aggregation). Further microstructural analysis after shearing is recommended to examine more

closely the influence of the degree of particle aggregation on the observed G/G_0 and D/D_0 responses at rather high strains.

CONCLUSIONS

Based on the experimental study, it is found that the maximum shear modulus G_0 increases with increasing suction for both NL and GL. The increase rate for GL is larger than NL by about 10%. This difference is likely attributed to their different degrees of aggregation. SEM images reveal that NL consists of larger aggregations whereas GL is made up of many smaller aggregations. The larger aggregation of NL is likely due to its higher contents of iron oxide, which enhances cladding of particles. Consequently, GL has a higher degree of saturation than NL at a given suction, resulting in more air-water interfaces which stiffen the soil skeleton.

With an increase in suction, the elastic threshold shear strain of lateritic clays becomes smaller. This observation implies that if the stiffness degradation characteristics of unsaturated lateritic soils are only determined at saturated condition, the elastic threshold shear strain would be overestimated. Consequently, the stiffness reduction and hence soil deformation may be underestimated. Moreover, the observed trend is different from that of other fine-grained soils such as completely decomposed tuff (CDT), whose threshold shear strain is larger at a higher suction. The difference is likely because lateritic soil has more iron and aluminium oxides to enhance the formulation of aggregates. These aggregates shrink upon suction increases, resulting in larger inter-aggregates pores and thus a lower elastic threshold shear strain. For other fine-grained soils such as CDT, with an increase in suction, the water meniscuses increase the normal force and hence prevent slippage between the soil particles. Consequently, the elastic threshold shear strain becomes larger at a higher suction. This may also be due to micro-fissuring with suction increase. Further research is needed to explore the relation between microstructural features and elastic threshold strain value.

In terms of the initial damping ratio D_0, measured values range from 10% to 23% for NL and 11% to 14% for GL. These two soils have much larger D_0 than other soils such as compacted loess reported in the literature. The high D_0 values of lateritic soils are likely due to the presence of iron and/or aluminium sesquioxides, which promote the aggregation of particles.

The value of D_0 increases with an increase in suction. As suction increases from 0 to 300 kPa, the value of D_0 for NL and GL increases by 100% and 22%, respectively. It is clear that suction effects on NL are more significant than those on GL. The difference is likely because NL has larger aggregates caused by its iron oxide content. These larger aggregates shrink more and therefore result in a larger increment in D_0.

ACKNOWLEDGEMENTS

The authors would like to thank the Research Grants Council (RGC) of the HKSAR for providing financial support through the grants 16212218, 16204817 and AoE/E-603/18.

REFERENCES

Airey, D., Suchowerska, A., and Williams, D. 2012. Limonite – a weathered residual soil heterogeneous at all scales. Géotechnique Letters, **2**(3): 119–122. doi:10.1680/geolett.12.00026.

Ashmawy, A.K., Salgado, R., Guha, S., and Drnevich, V.P. 1995. Soil damping and its use in dynamic analyses. *In* Proceedings of 3rd International Conference on Recent Advances in Geotechnical Earthquake Engineering and Soil Dynamics. St. Louis, Missouri. pp. 35–41.

ASTM. 2017a. D6913/D6913M - 17: Standard Test Methods for Particle-Size Distribution (Gradation) of Soils Using Sieve Analysis. ASTM International, West Conshohocken, Pa. USA. doi:10.1520/D6913_D6913M-17.

ASTM. 2017b. D7928 - 17: Standard Test Method for Particle-Size Distribution (Gradation) of Fine-Grained Soils Using the Sedimentation (Hydrometer) Analysis. ASTM International, West Conshohocken, Pa. USA. doi:10.1520/D7928-17.

ASTM. 2017c. D2487 − 17′1: Standard Practice for Classification of Soils for Engineering Purposes (Unified Soil Classification System). ASTM International, West Conshohocken, Pa. USA. doi:10.1520/D2487-17E01.

Blight, G.E. 1991. Theme lecture: Tropical processes causing rapid geological change. Geological Society, London, Engineering Geology Special Publications, **7**(1): 459–471. doi:10.1144/GSL.ENG.1991.007.01.43.

Borden, R.H., Shao, L., and Gupta, A. 1996. Dynamic Properties of Piedmont Residual Soils. Journal of Geotechnical Engineering, **122**(10): 813–821. American Society of Civil Engineers. doi:10.1061/(ASCE)0733-9410(1996)122:10(813).

Cha, M., Santamarina, J.C., Kim, H.-S., and Cho, G.-C. 2014. Small-Strain Stiffness, Shear-Wave Velocity, and Soil Compressibility. Journal of Geotechnical and Geoenvironmental Engineering, **140**(10): 06014011-1–4. doi:10.1061/(asce)gt.1943-5606.0001157.

Clayton, C.R.I., and Heymann, G. 2001. Stiffness of geomaterials at very small strains. Géotechnique, **51**(3): 245–255. doi:10.1680/geot.2001.51.3.245.

Dobry, R., and Vucetic, M. 1987. Dynamic properties and seismic response of soft clay deposits. Proc. Int. Symp. on Geotechnical Engineering of Soft Soils, **2**: 51-87. Department of Civil Engineering, Rensselaer Polytechnic Institute.

Fredlund, D.G., and Xing, A. 1994. Equations for the soil-water characteristic curve. Canadian Geotechnical Journal, **31**(4): 521–532. doi:10.1139/t94-061.

Gidigasu, M.D. 1976. Laterite Soil Engineering - Pedogenesis and Engineering Principles. *In*

Elsevier Scientific Pub. Co. Amsterdam. doi:10.1016/B978-0-444-41283-6.50005-8.

Goldberg, S. 1989. Interaction of aluminum and iron oxides and clay minerals and their effect on soil physical properties: A review. Communications in Soil Science and Plant Analysis, **20**(11–12): 1181–1207. doi:10.1080/00103629009368144.

Hardin, B.O., and Black, W.L. 1966. Sand stiffness under various triaxial stresses. Journal of Soil Mechanics & Foundations Div, **92**(2): 27–42.

Heitor, A., Indraratna, B., and Rujikiatkamjorn, C. 2013. Laboratory study of small-strain behavior of a compacted silty sand. Canadian Geotechnical Journal, **50**(2): 179–188. doi:10.1139/cgj-2012-0037.

Hoyos, L.R., and Puppala, A.J. 2017. Experimental Modeling of Unsaturated Intermediate Geomaterials for Sustainable Design of Geotechnical Infrastructure. *Edited by* G.L. Sivakumar Babu, S. Saride, and B.M. Basha. Springer, Singapore, Singapore. pp. 175–197. doi:10.1007/978-981-10-1930-2_11.

Hoyos, L.R., Suescún-Florez, E.A., and Puppala, A.J. 2015. Stiffness of intermediate unsaturated soil from simultaneous suction-controlled resonant column and bender element testing. Engineering Geology, **188**: 10–28. Elsevier. doi:10.1016/j.enggeo.2015.01.014.

Kallioglou, P., Tika, T.H., and Pitilakis, K. 2008. Shear modulus and damping ratio of cohesive soils. Journal of Earthquake Engineering, **12**(6): 879–913.

Khosravi, A., and McCartney, J.S. 2012. Impact of Hydraulic Hysteresis on the Small-Strain Shear Modulus of Low Plasticity Soils. Journal of Geotechnical and Geoenvironmental Engineering, **138**(11): 1326–1333. doi:10.1061/(ASCE)GT.1943-5606.0000713.

Khosravi, A., Shahbazan, P., and Pak, A. 2018. Impact of hydraulic hysteresis on the small

strain shear modulus of unsaturated sand. Soils and Foundations, **58**(2): 344–354. doi:10.1016/j.sandf.2018.02.018.

Li, X.S., Yang, W.L., Shen, C.K., and Wang, W.C. 1998. Energy-Injecting Virtual Mass Resonant Column System. Journal of Geotechnical and Geoenvironmental Engineering, **124**(5): 428–438. doi:10.1061/(ASCE)1090-0241(1998)124:5(428).

Lyon Associates, I., and BRRI. 1971. Laterite and lateritic soils and other problem soils of Africa. Baltimore, Maryland, U.S.A.

Mancuso, C., Silvestri, F., and Vinale, F. 1993. Stress-strain behavior of a damcore material by field and laboratory dynamic tests. *In* Proceedings of the International Symposium Geotechnical Engineering of Hard Soils-Soft Rocks, Rotterdam: Balkema. pp. 1299–1308.

Mancuso, C., Vassallo, R., and D'Onofrio, A. 2002. Small strain behavior of a silty sand in controlled-suction resonant column - torsional shear tests. Canadian Geotechnical Journal, **39**(1): 22–31. doi:10.1139/t01-076.

Miguel, M.G., and Bonder, B.H. 2012. Soil-Water Characteristic Curves Obtained for a Colluvial and Lateritic Soil Profile Considering the Macro and Micro Porosity. Geotechnical and Geological Engineering, **30**(6): 1405–1420. doi:10.1007/s10706-012-9545-y.

Netterberg, F. 2014. Review of specification for the use of laterite in road pavements. Contract AFCAP/GEN/124: Association of Southern Africa National Road Agency, UK Department of International Development.

Ng, C.W.W., Akinniyi, D.B., Zhou, C., and Chiu, C.F. 2019. Comparisons of weathered lateritic, granitic and volcanic soils: Compressibility and shear strength. Engineering

Geology, **249**: 235–240. Elsevier B.V. doi:10.1016/j.enggeo.2018.12.029.

Ng, C.W.W., Baghbanrezvan, S., Sadeghi, H., Zhou, C., and Jafarzadeh, F. 2017. Effect of specimen preparation techniques on dynamic properties of unsaturated fine-grained soil at high suctions. Canadian Geotechnical Journal, **54**(9): 1310–1319. doi:10.1139/cgj-2016-0531.

Ng, C.W.W., and Xu, J. 2012. Effects of current suction ratio and recent suction history on small-strain behaviour of an unsaturated soil. Canadian Geotechnical Journal, **49**(2): 226–243. doi:10.1139/t11-097.

Ng, C.W.W., Xu, J., and Yung, S.Y. 2009. Effects of wetting–drying and stress ratio on anisotropic stiffness of an unsaturated soil at very small strains. Canadian Geotechnical Journal, **46**(9): 1062–1076. doi:10.1139/T09-043.

Ng, C.W.W., and Yung, S.Y. 2008. Determination of the anisotropic shear stiffness of an unsaturated decomposed soil. Géotechnique, **58**(1): 23–35. doi:10.1680/geot.2008.58.1.23.

Pineda, J.A., Colmenares, J.E., and Hoyos, L.R. 2014. Effect of Fabric and Weathering Intensity on Dynamic Properties of Residual and Saprolitic Soils via Resonant Column Testing. Geotechnical Testing Journal, **37**(5): 800–816. doi:10.1520/GTJ20120132.

Romero, E. 2013. A microstructural insight into compacted clayey soils and their hydraulic properties. Engineering Geology, **165**: 3–19. doi:10.1016/j.enggeo.2013.05.024.

Sawangsuriya, A., Edil, T.B., and Bosscher, P.J. 2008. Modulus−suction−moisture relationship for compacted soils. Canadian Geotechnical Journal, **45**(7): 973–983. doi:10.1139/T08-033.

Sawangsuriya, A., Edil, T.B., and Bosscher, P.J. 2009. Modulus-suction-moisture relationship

for compacted soils in postcompaction state. Journal of Geotechnical and geoenvironmental engineering, **135**(10): 1390–1403.

Seed, H.B., Wong, R.T., Idriss, I.M., and Tokimatsu, K. 1986. Moduli and damping factors for dynamic analyses of cohesionless soils. Journal of geotechnical engineering, **112**(11): 1016–1032. American Society of Civil Engineers.

Senetakis, K., Anastasiadis, A., and Pitilakis, K. 2013. Normalized shear modulus reduction and damping ratio curves of quartz sand and rhyolitic crushed rock. Soils and Foundations, **53**(6): 879–893. doi:10.1016/j.sandf.2013.10.007.

Shankar Kumar, S., Murali Krishna, A., and Dey, A. 2014. Parameters Influencing Dynamic Soil Properties: A Review Treatise. International Journal of Innovative Research in Science, **3**(4): 47–60. Available from www.ijirset.com.

Simpson, B. 1992. Retaining structures: displacement and design. Géotechnique, **42**(4): 541–576. doi:10.1680/geot.1992.42.4.541.

Tawiah, S.O. 2019. A Laboratory Study on the Microstructural and Hydro-mechanical Behaviour of Unsaturated Lateritic Soils. M.Phil Thesis. The Hong Kong University of Science and Technology, Clear Water Bay, Kowloon, Hong Kong.

Tzyy-Shiou, C., RamaKumar, V. V, and Kuo-Ping, C. 2001. Improvement of Static and Dynamic Properties of Soft Clay Using High Pressure Jet Grout. *In* International Conference on Recent Advances in Geotechnical Earthquake Engineering and Soil Dynamics. University of Missouri--Rolla.

Upreti, K., Leong, E., Ph, D., and Asce, M. 2017. Dynamic Properties of Residual Soil over a Wide Range of Strain. PanAm Unsaturated Soils 2017,: 388–397. American Society of Civil Engineers, Reston, VA. doi:10.1061/9780784481707.039.

Vardanega, P.J., and Bolton, M.D. 2013. Stiffness of clays and silts: Normalizing shear modulus and shear strain. Journal of Geotechnical and Geoenvironmental Engineering, **139**(9): 1575–1589.

Vassallo, R., Mancuso, C., and Vinale, F. 2007. Effects of net stress and suction history on the small strain stiffness of a compacted clayey silt. Canadian Geotechnical Journal, **44**(4): 447–462. doi:10.1139/t06-129.

Vinale, F., D'Onofrio, A., Mancuso, C., Santucci de Magistris, F., and Tatsuoka, F. 1999. The pre-failure behaviour of soils as construction materials. *In* Proceedings of the 2nd International Symposium on Pre-failure Deformation Characteristics of Geomaterials. A. A. Balkema, Torino, Italy. pp. 955–1007.

Vucetic, M. 1994. Cyclic threshold shear strains in soils. Journal of Geotechnical Engineering, **120**(12): 2208–2228.

Vucetic, M., and Dobry, R. 1991. Effect of Soil Plasticity on Cyclic Response. Journal of Geotechnical Engineering, **117**(1): 89–107. doi:10.1061/(ASCE)0733-9410(1991)117:1(89).

Wheeler, S.J., and Karube, D. 1996. Constitutive modelling. *In* Proceedings 1st International Conference on Unsaturated Soil, Paris. *Edited by* P. Alonso, E.E. & Delage. Rotterdam, the Netherlands: Balkema. pp. 1323–1356.

Wheeler, S.J., Sharma, R.S., and Buisson, M.S.R. 2003. Coupling of hydraulic hysteresis and stress–strain behaviour in unsaturated soils. Géotechnique, **53**(1): 41–54. doi:10.1680/geot.2003.53.1.41.

Wu, S., Gray, D.H., and Richart Jr, F.E. 1984. Capillary effects on dynamic modulus of sands and silts. Journal of Geotechnical Engineering, **110**(9): 1188–1203.

Xenaki, V.C., and Athanasopoulos, G.A. 2008. Dynamic properties and liquefaction resistance of two soil materials in an earthfill dam—Laboratory test results. Soil Dynamics and Earthquake Engineering, **28**(8): 605–620. doi:10.1016/j.soildyn.2007.10.001.

Zhang, X.W., Kong, L.W., Cui, X.L., and Yin, S. 2016. Occurrence characteristics of free iron oxides in soil microstructure: evidence from XRD, SEM and EDS. Bulletin of Engineering Geology and the Environment, **75**(4): 1493–1503. doi:10.1007/s10064-015-0781-2.

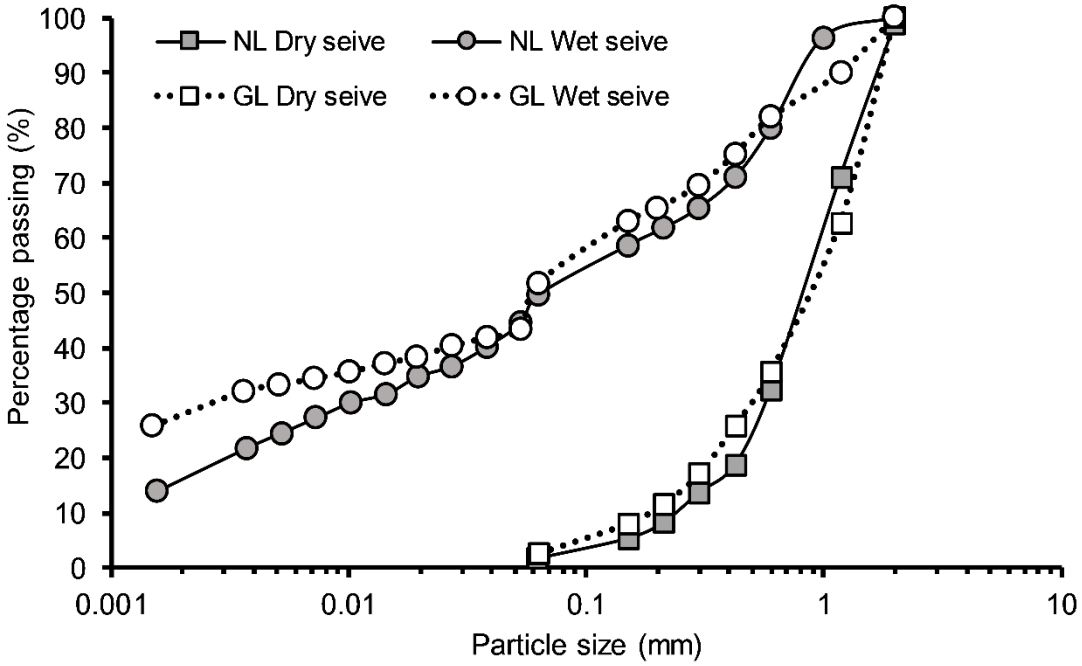

Figure 1 Particle size distributions of two lateritic soils

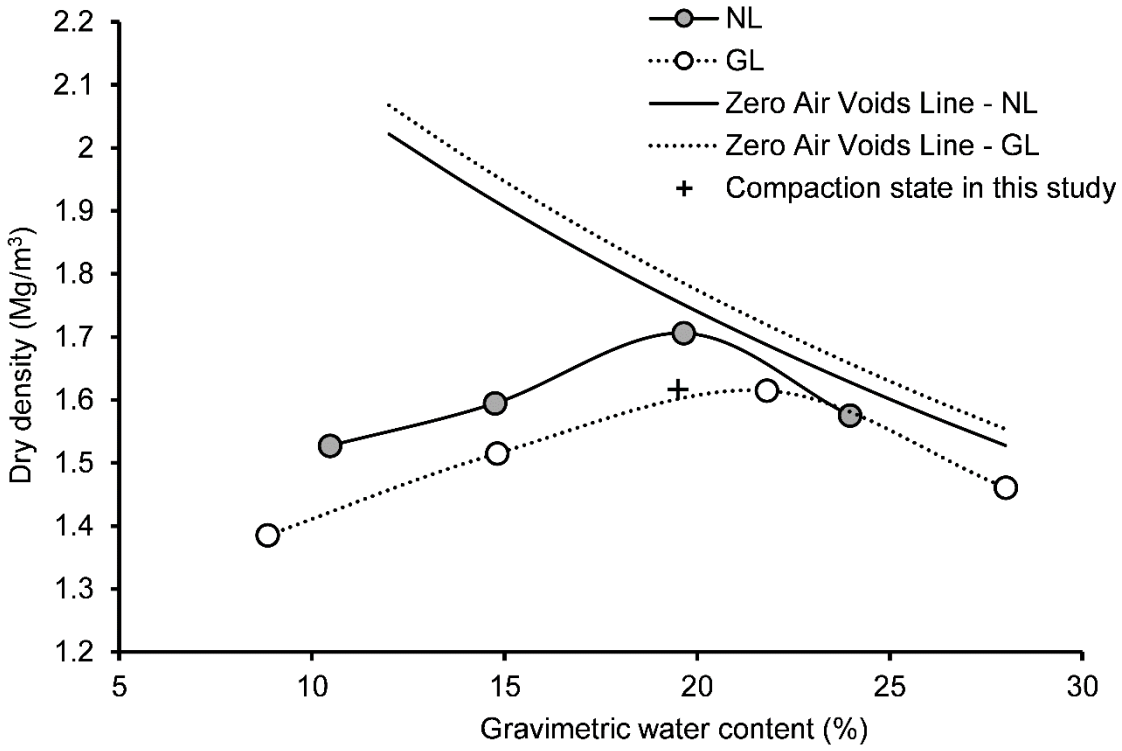

Figure 2 Compaction curve of two lateritic soils

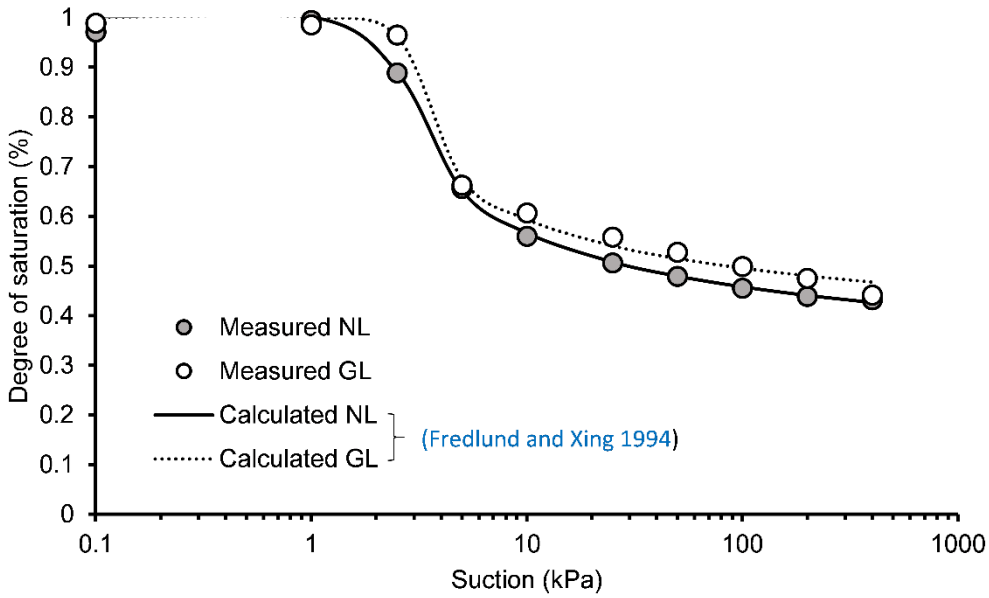

Figure 3 Water retention curves of two lateritic soils after Tawiah (2019)

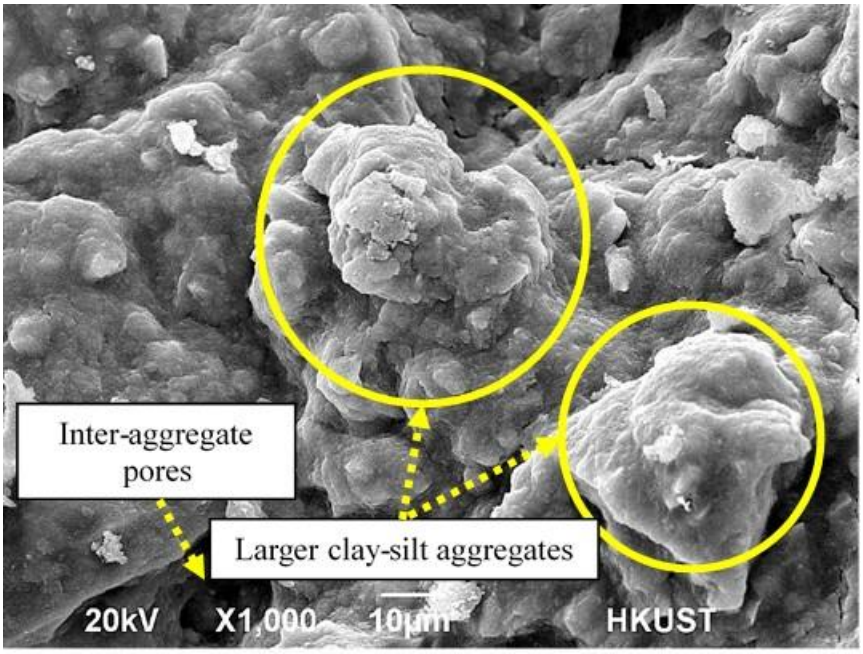
Inter-aggregate pores
Larger clay-silt aggregates
20kV X1,000 10μm HKUST

(a)

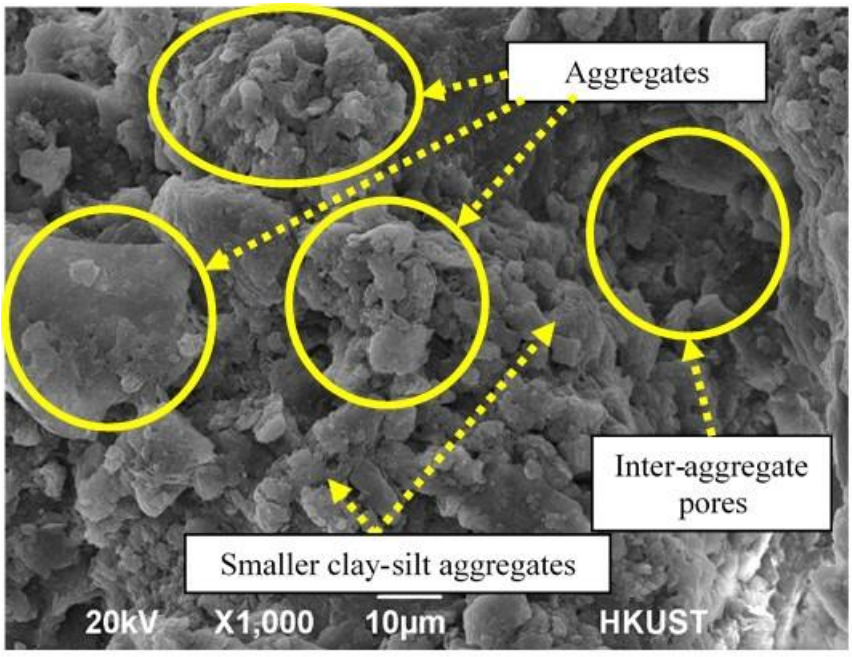
Aggregates
Inter-aggregate pores
Smaller clay-silt aggregates
20kV X1,000 10μm HKUST

(b)

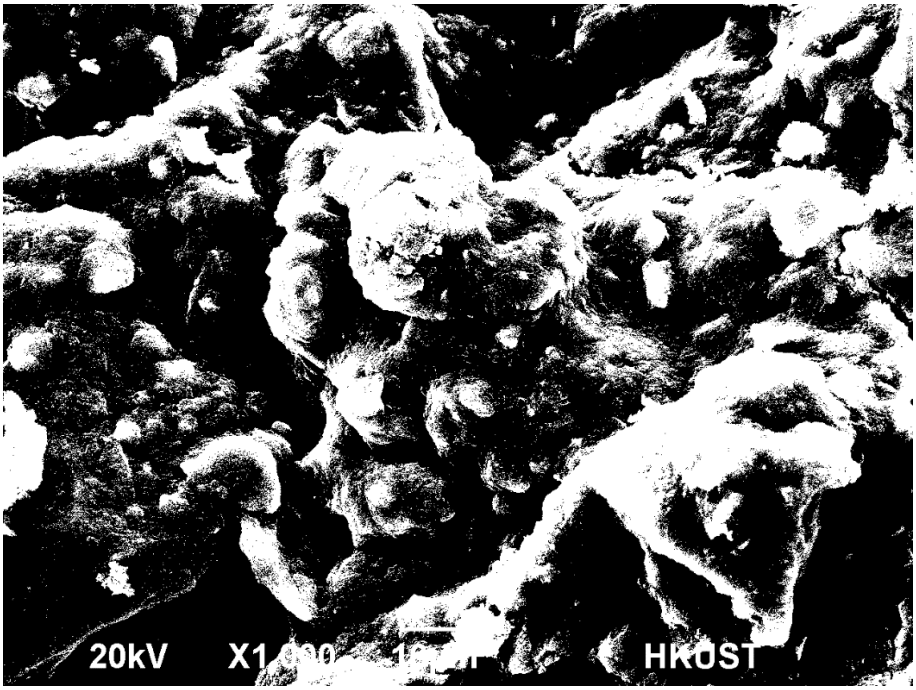

(c)

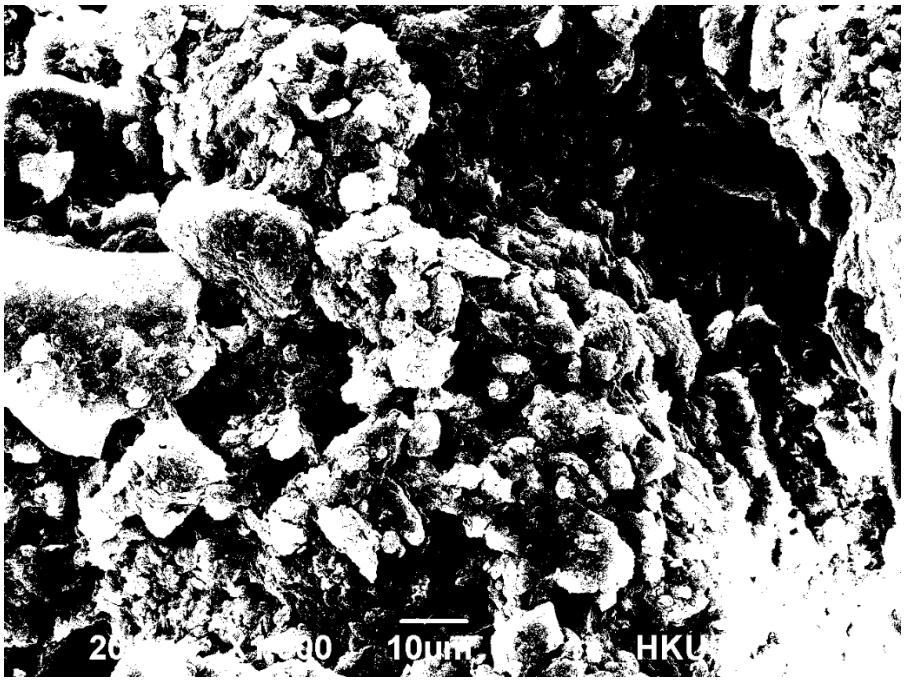

(d)

Figure 4 SEM images of (a) NL (b) GL (c) NL binarized (d) GL binarized

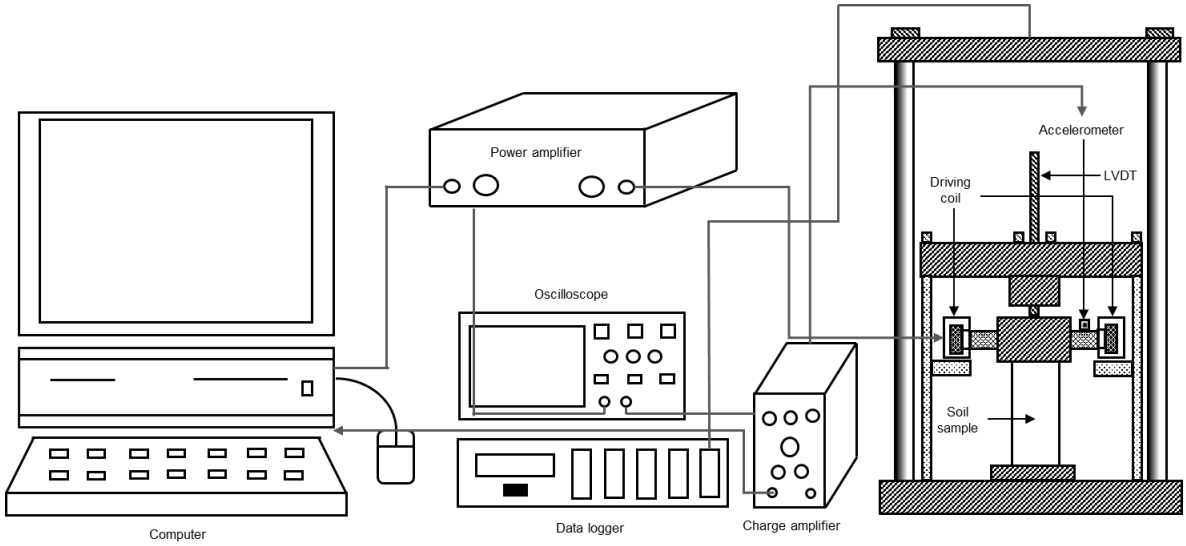

Figure 5 Schematic diagram of energy injecting resonant column apparatus after Li et al. (1998)

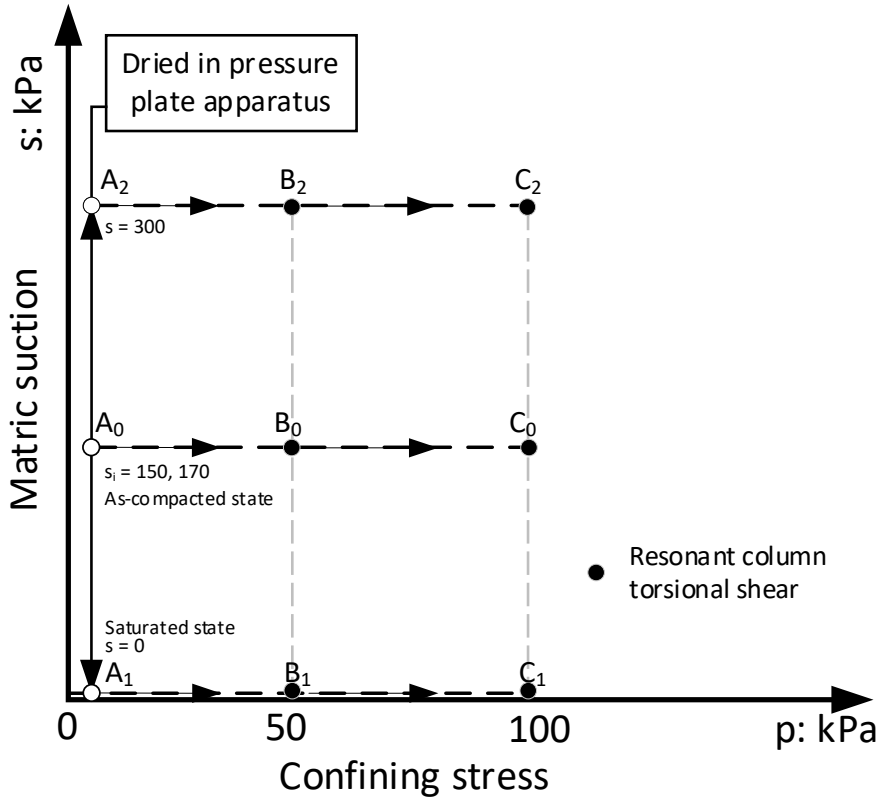

Figure 6 Stress paths carried out in resonant column tests

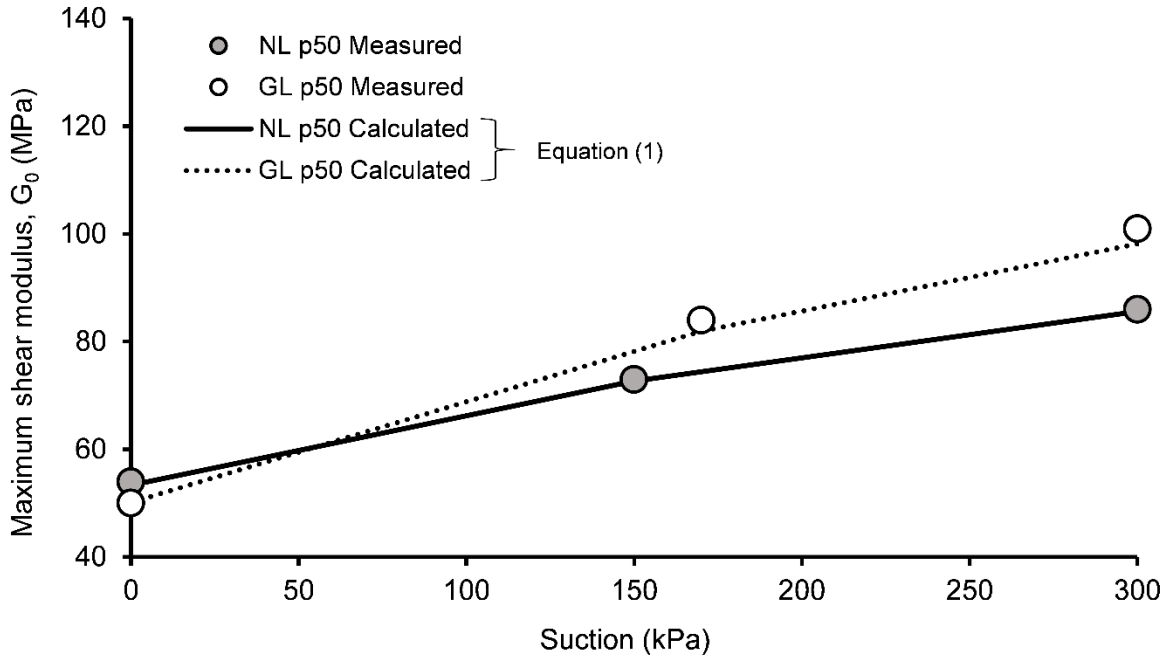

(a)

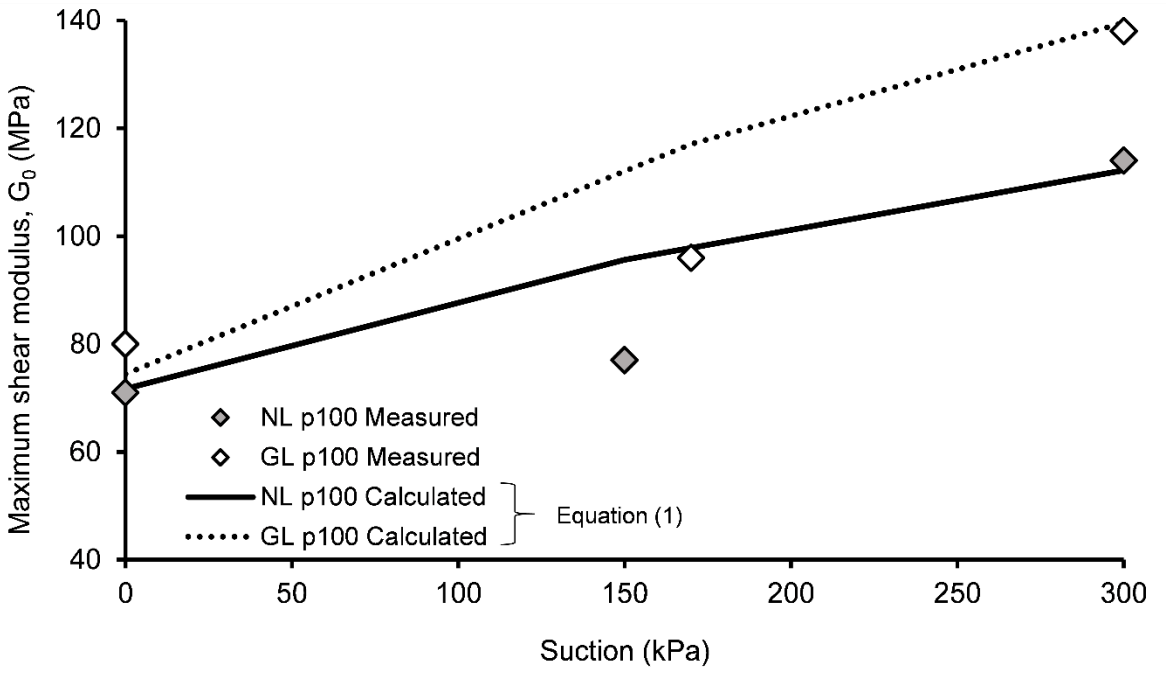

(b)

Figure 7 Measured and calculated G_0 values at different suction values and confining stresses of (a) 50 kPa and (b) 100 kPa

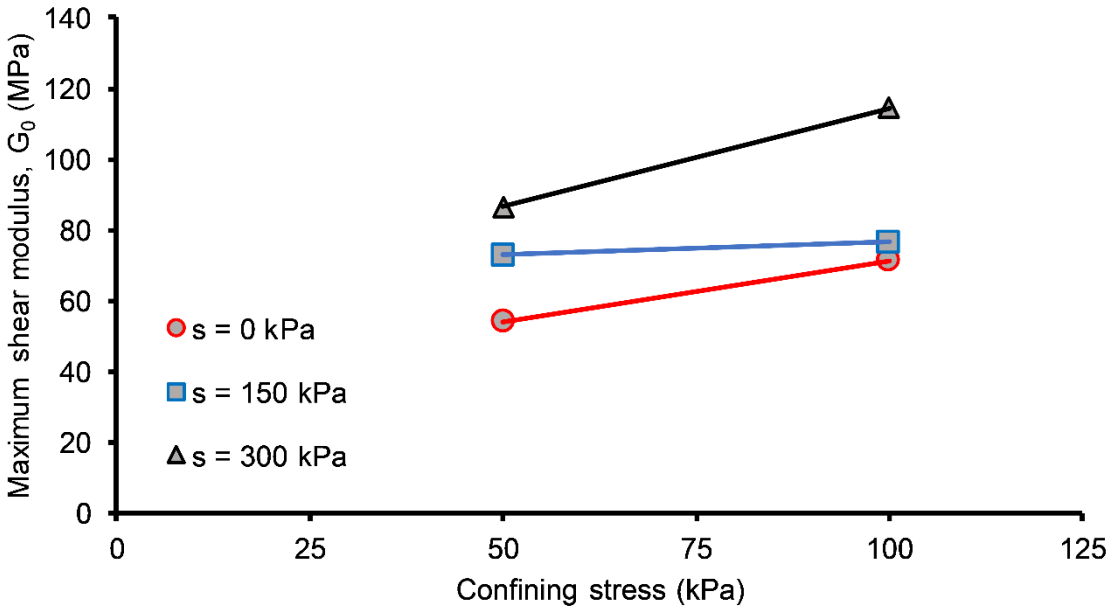

(a)

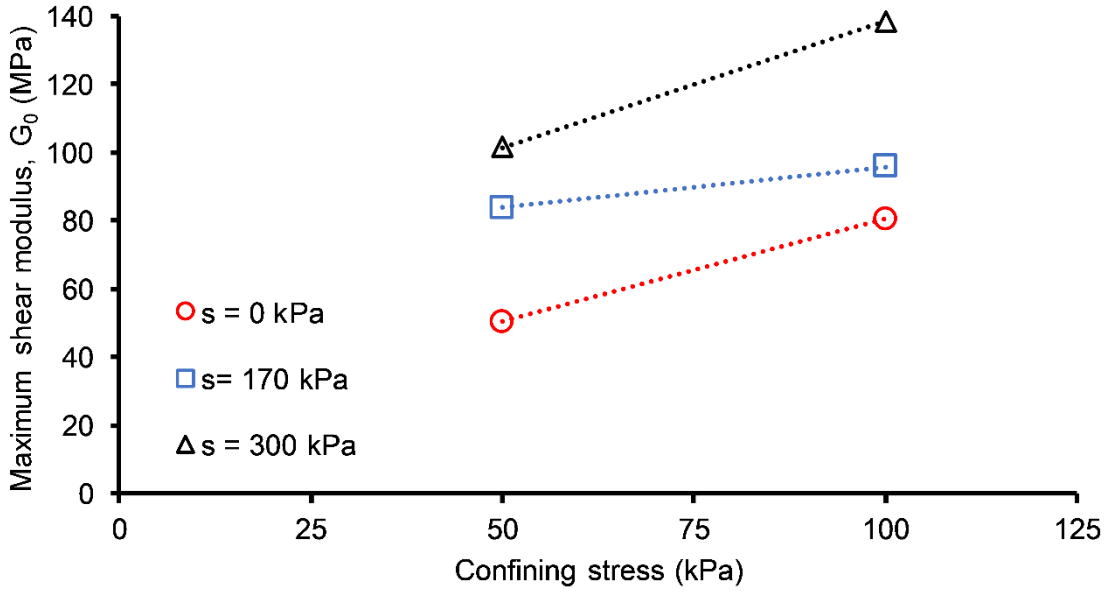

(b)

Figure 8 Relationships between G_0 and confining stress at various suctions: (a) NL and (b) GL

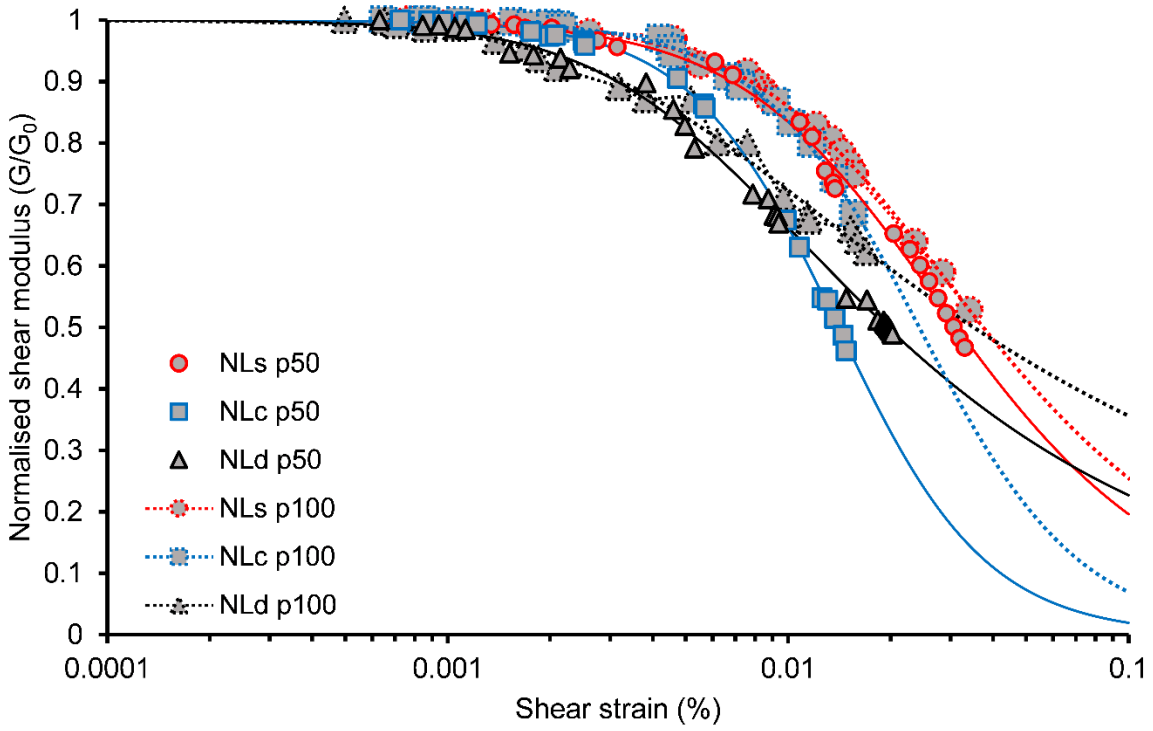

(a)

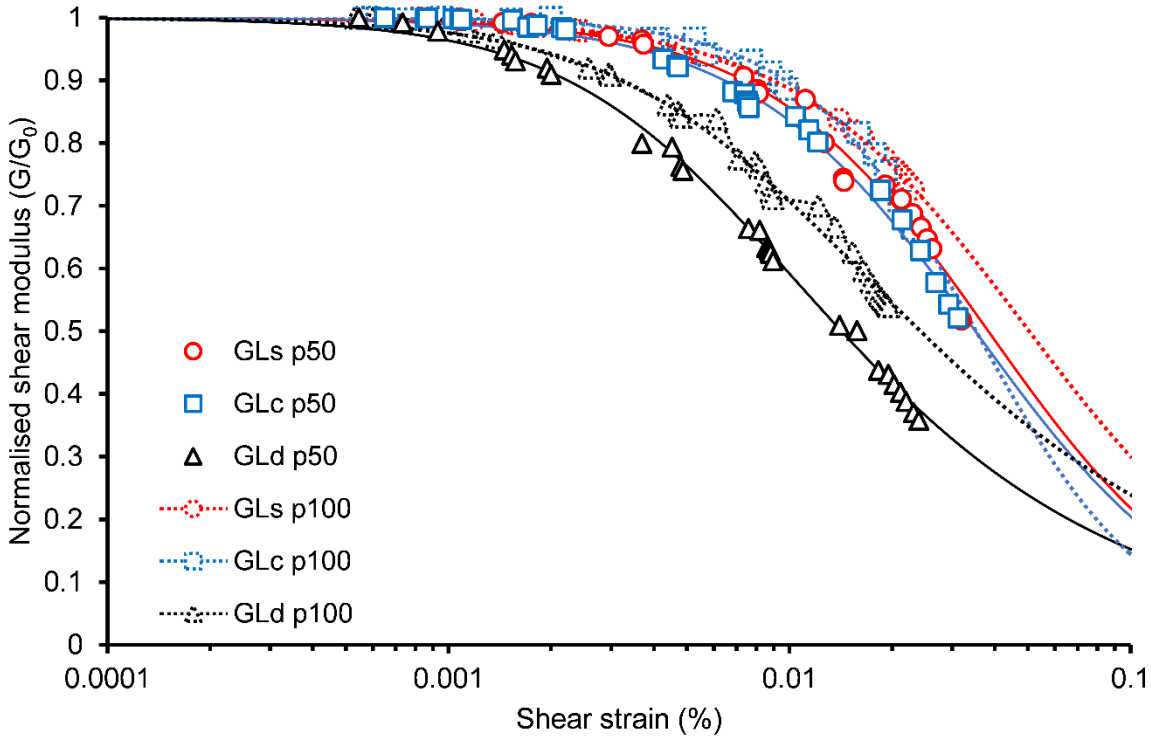

(b)

Figure 9 Normalised shear modulus degradation curves for (a) NL and (b) GL

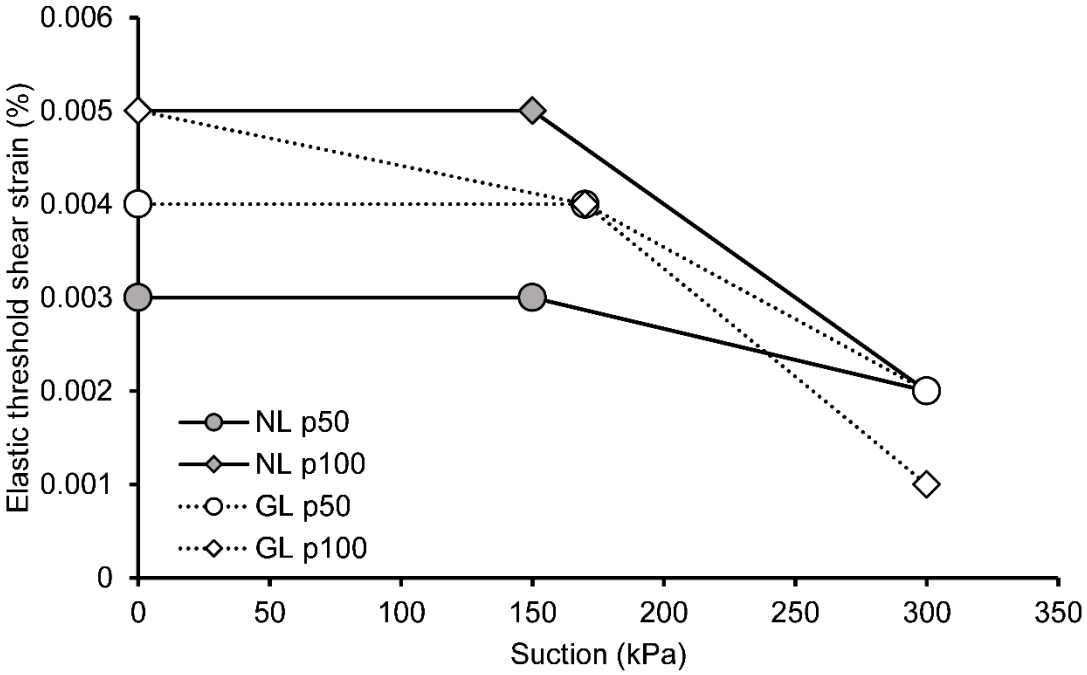

Figure 10 Changes of elastic threshold shear strain with suction

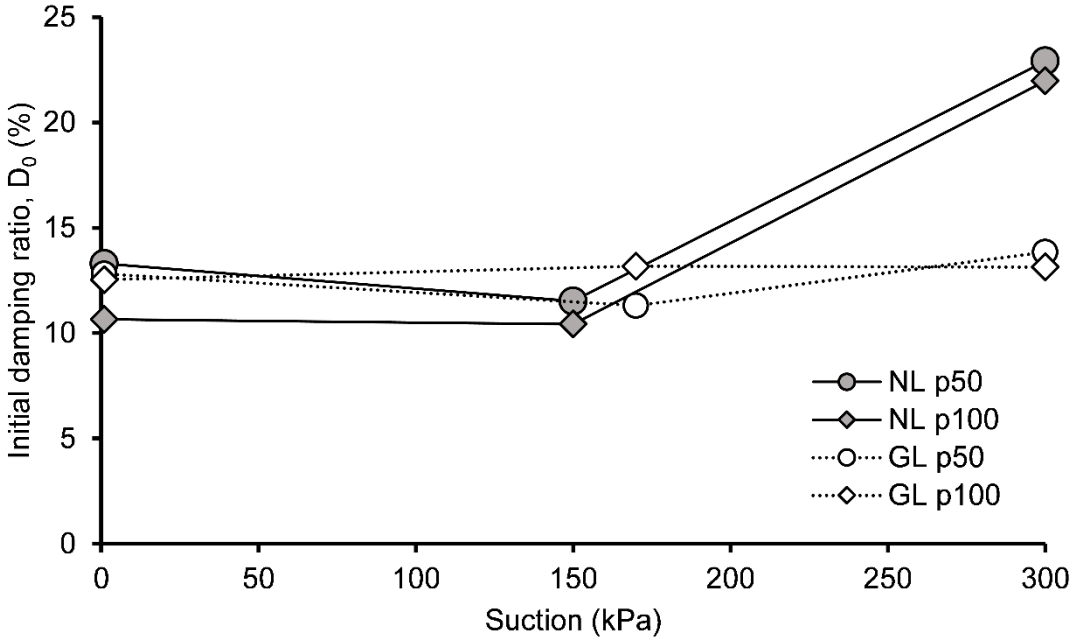

Figure 11 Changes of initial damping ratio with suction for NL and GL

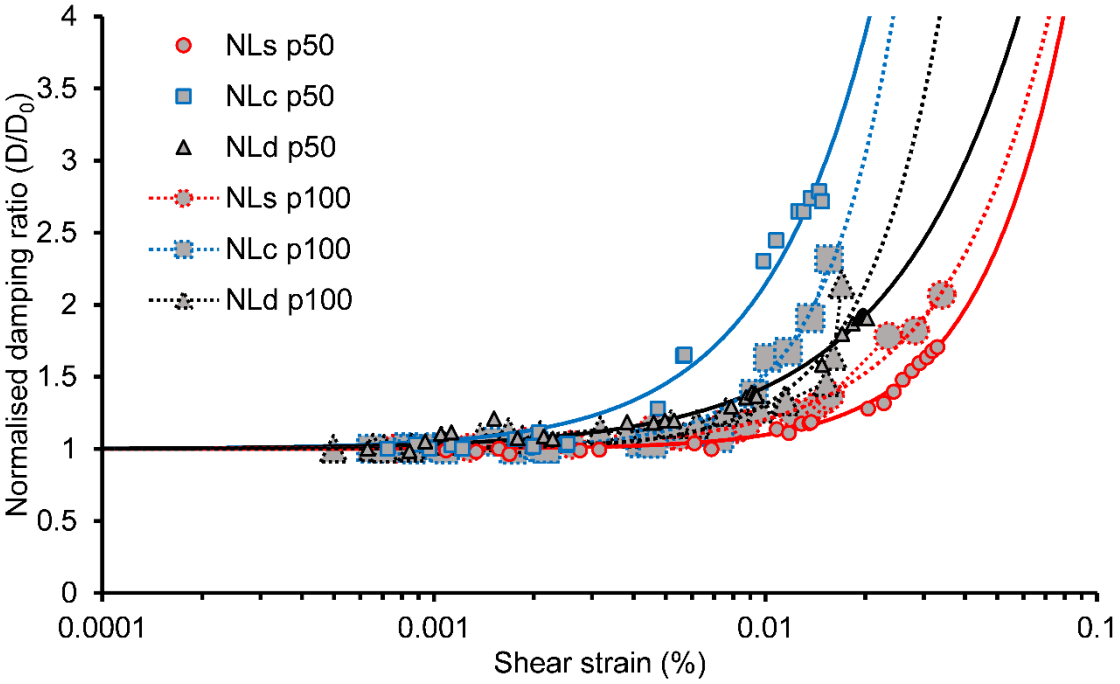

(a)

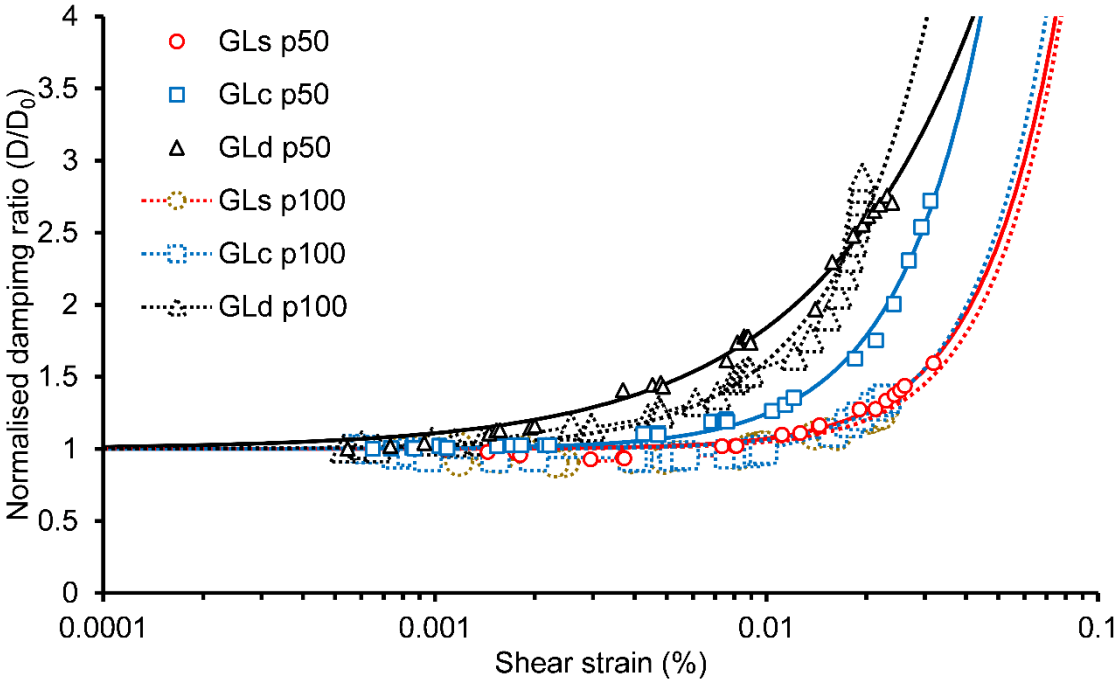

(b)

Figure 12 Normalised damping ratio curves for (a) NL and (b) GL

Table 1 Physical properties of the lateritic soils

Index test	NL*	GL*
Atterberg limits		
Liquid limit	47	54
Plasticity index	21	32
Particle size distribution (%)		
Sand fraction	50	48
Silt fraction	36	26
Clay fraction	14	26
Standard Proctor compaction		
Optimum moisture content (%)	19.5	21.2
Maximum dry density (Mg/m^3)	1.702	1.612
Classification		
USCS (ASTM 2017)	Sandy lean clay (CL)	Sandy fat clay (CH)
Main chemical composition (%)		
SiO_2	60	62
Fe_2O_3	10	4
Al_2O_3	28	32

*Note: *NL*: Lateritic soil from Nigeria; *GL*: Lateritic soil from Ghana

Table 2 Testing programme and soil state prior to resonant column test

Specimen ID*	Suction, s: kPa	Confining pressure, p: kPa	Void ratio before compression, e_0	Void ratio after compression, e_f	Water content, w: %	Degree of saturation, S_r
NLs p50	0	50	0.652	0.647	24.3	0.99
NLc p50	150		0.651	0.648	19.5	0.80
NLd p50	300		0.651	0.646	16.5	0.68
NLs p100	0	100	0.649	0.629	23.6	0.98
NLc p100	150		0.651	0.642	19.5	0.81
NLd p100	300		0.651	0.638	16.5	0.69
GLs p50	0	50	0.652	0.653	23.7	1
GLc p50	170		0.652	0.645	19.5	0.83
GLd p50	300		0.651	0.649	17.9	0.76
GLs p100	0	100	0.652	0.626	22.8	1
GLc p100	170		0.651	0.639	19.5	0.84
GLd p100	300		0.650	0.646	17.9	0.76

*Note: *NL*: Lateritic soil from Nigeria; *GL*: Lateritic soil from Ghana; s: saturated c: as-compacted state with a water content of 19.5%; d: drying in a pressure plate apparatus to 300 kPa suction.

Table 3 Summary of measured & calculated parameters of stiffness and damping ratio

Specimen ID	C_{ij}	n	b	Measured G_0	Calculated G_0	Measured elastic threshold shear strain, $G/G_0 = 0.95$	Measured D_0 (%)
NLs p50	310	0.19	0.17	54	53	0.003	13.3
NLc p50				73	73	0.003	11.5
NLd p50				86	86	0.002	22.9
NLs p100				71	72	0.005	10.7
NLc p100				77	96	0.005	10.4
NLd p100				114	112	0.002	22.0
GLs p50	320	0.25	0.24	50	50	0.004	12.8
GLc p50				84	79	0.004	11.3
GLd p50				101	98	0.002	13.8
GLs p100				80	74	0.005	12.5
GLc p100				96	113	0.004	13.2
GLd p100				138	140	0.001	13.1